AIP Journal of Applied Physics

Homeotropic alignment and Förster resonance energy transfer: The way to a brighter luminescent solar concentrator

Clemens Tummeltshammer, Alaric Taylor, Anthony J. Kenyon, and Ioannis Papakonstantinou

Citation: Journal of Applied Physics **116**, 173103 (2014); doi: 10.1063/1.4900986
View online: http://dx.doi.org/10.1063/1.4900986
View Table of Contents: http://scitation.aip.org/content/aip/journal/jap/116/17?ver=pdfcov
Published by the AIP Publishing

Homeotropic alignment and Förster resonance energy transfer: The way to a brighter luminescent solar concentrator

Clemens Tummeltshammer, Alaric Taylor, Anthony J. Kenyon, and Ioannis Papakonstantinou[a)]
Department of Electronic and Electrical Engineering, University College London, London WC1E 7JE, United Kingdom

(Received 7 July 2014; accepted 22 October 2014; published online 4 November 2014)

We investigate homeotropically aligned fluorophores and Förster resonance energy transfer (FRET) for luminescent solar concentrators using Monte-Carlo ray tracing. The homeotropic alignment strongly improves the trapping efficiency, while FRET circumvents the low absorption at homeotropic alignment by separating the absorption and emission processes. We predict that this design doped with two organic dye molecules can yield a 82.9% optical efficiency improvement compared to a single, arbitrarily oriented dye molecule. We also show that quantum dots are prime candidates for absorption/donor fluorophores due to their wide absorption band. The potentially strong re-absorption and low quantum yield of quantum dots is not a hindrance for this design.
 [http://dx.doi.org/10.1063/1.4900986]

I. INTRODUCTION

Luminescent solar concentrators (LSCs) have the potential to enhance the economic viability of solar energy.[1,2] They concentrate both direct and diffuse incoming sunlight and, thus, need no expensive tracking equipment. LSCs consist of a flat waveguide doped with fluorophores that absorb the incoming sunlight and re-emit it at a longer wavelength. Depending on the angle of re-emission, photons are trapped due to total internal reflection and guided towards the side surfaces of the waveguide. Solar cells fixed to the side surfaces will then convert photons into electricity.

Since their inception in the late 70s,[3–5] LSCs have been struggling with the following deficiencies: escape cone losses, re-absorption losses, and limited spectral efficiency. As dye molecules are generally arbitrarily oriented within the host matrix, the angularly averaged emission from the dye population can be assumed to be isotropic. As a result, for a host matrix with a refractive index of 1.5, about 25% of the power will be emitted within the escape cone and leave the waveguide. Additionally, absorption and emission spectra of fluorophores often overlap; therefore, emitted photons could be re-absorbed. This increases losses due to a non-unity quantum yield and escape cone losses. Finally, the spectral band of fluorophores often only covers a small wavelength band within the AM1.5G spectrum.

There have been different approaches to circumvent these losses, such as wavelength-selective mirrors,[6–8] plasmonics,[9–12] or alternative fluorophores.[13] Recently, it was also shown that aligning the dye molecules with the help of a liquid crystal can lead to a higher trapping efficiency and, thus, lower escape cone losses.[14–18] Previous experiments indicate that the aggregated escape cone losses account for a photon loss of 50% to 70% for a $50 \times 50 \times 3\,\mathrm{mm}^3$ LSC.[19] By aligning the polarizability axis of the dye molecule normal to the top surface, i.e., homeotropic alignment, the escape cone losses of a single emission event can be reduced from about 25% (random dye orientation) to 9% (perfectly aligned) for a waveguide with refractive index of 1.5.[17] This reduction to the single emission event should result in significant reductions to the aggregated escape cone losses. However, at a high degree of homeotropic alignment, the absorption of incoming light is strongly reduced. Therefore, it was suggested to add a second dye to the LSC that absorbs the incoming light more efficiently and transfers the energy to the homeotropically aligned dye through Förster resonance energy transfer (FRET).[15,20–22] The advanced two-dye LSC is shown in Fig. 1 with the homeotropically aligned dye (acceptor) linked to either one (a) or two (b) absorption dyes (donor).

This paper is the first, to our knowledge, to investigate the potential of this two-dye system using modeling. We have developed a Monte-Carlo ray tracing tool that incorporates FRET and dye alignment and can compute the

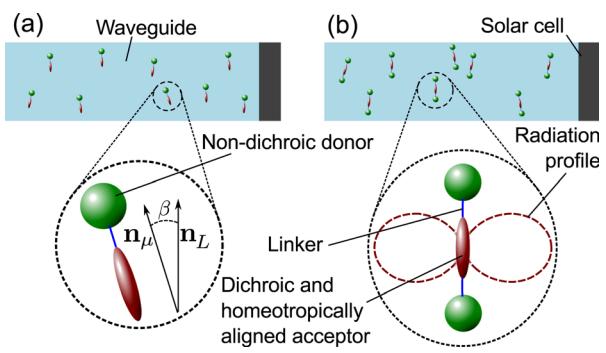

FIG. 1. Two-dye system LSC with a non-dichroic donor/absorption dye and a homeotropically aligned acceptor/emission dye. Each acceptor dye is linked to (a) one or (b) two donor dyes. The angle between the polarizability axis of the acceptor $\mathbf{n}_\mu$ and the liquid crystal director $\mathbf{n}_L$ is given by β.

[a)]Author to whom correspondence should be addressed. Electronic mail: i.papakonstantinou@ucl.ac.uk

efficiency of this LSC design. Due to the size and design of LSCs, ray tracing is the dominant method to model LSCs.[5,23–25] With our tool, we can determine the optimal (1) dye concentration, (2) distance between the two types of dye molecules, (3) absorption peaks separation between the absorption and emission dye, and (4) quality of homeotropic alignment. Optimizing all these parameters experimentally would be a time consuming and expensive process; therefore, we opted to simulate the LSC system before verifying our results experimentally. We show that the theoretical efficiency of a dye-doped LSC can be enhanced by up to 82.9% by utilizing FRET and dye alignment. The design becomes even more efficient by using a quantum dot as absorption fluorophore due to the quantum dot's wide absorption band. Additionally, deficiencies of quantum dots such as low quantum yield and high re-absorption are circumvented by the design.

Section II describes the theoretical background of aligned and dichroic dye molecules and FRET. The Monte-Carlo ray tracer is described in Sec. III. The results are presented in Sec. IV. First, the parameters of the two-dye system are optimized and, then, compared to a single dye system for various LSC sizes. Subsequently, the importance of the quantum yield and quantum dots doped LSCs are investigated. In Sec. V, we draw conclusions about the potential of this design for optimizing LSC efficiency.

II. THEORY

To enhance the trapping efficiency and thereby reduce escape cone losses, the dye molecules not only have to be well aligned but also need to be dichroic. A dichroic dye molecule exhibits anisotropic absorption and emission. The former is due to a preferred axis of absorption. This means the strength of light absorption is dependent on the orientation of the electric field vector. A perfectly dichroic fluorophore would be equivalent to a dipole, which is polarizable only along one axis. The power absorbed by a dipole is proportional to $P_{\text{abs}} \propto |\mathbf{n}_\mu \cdot \mathbf{n}_E|^2$, where $\mathbf{n}_\mu$ and $\mathbf{n}_E$ are the unit vectors in the directions of the polarizability axis of the dipole and the electric field vector at the location of the dipole, respectively.[26] As a result, little absorption would occur for homeotropically oriented dye molecules and normally incident light, as the electric field and the polarization axis would be close to normal to each other.

Similarly, the power radiated by a dipole per unit solid angle $\mathrm{d}P_{\text{rad}}/\mathrm{d}\Omega$ is dependent on the orientation of the polarizability axis. It is proportional to $\sin(\alpha)^2$, where α is the angle between the polarizability axis $\mathbf{n}_\mu$ and the direction of emission.[27] It is indeed the $\sin^2$ dependence that ensures the higher trapping efficiency for homeotropic alignment.

The molecules of a liquid crystal align along a common axis, the director, which promotes alignment of dye molecules. However, dye molecules are generally not perfectly dichroic, and the alignment of the dye molecules within the liquid crystal host might slightly deviate from the director of the liquid crystal host.[14] To incorporate this, we average the absorption and emission profile of a dipole over a range of orientations. A single dye molecule's orientation probability might not be normally distributed; however, for the vast number of dye molecules within a LSC, the distribution of the average will converge to a normal distribution as stated by the central limit theorem.[28] Thus, we assume that the dipole orientation probability is

$$\Pr(\beta|\sigma) \propto \frac{1}{\sigma\sqrt{2\pi}} \exp\left(\frac{-\beta}{2\sigma^2}\right) \quad 0 \le \beta \le \pi, \tag{1}$$

where β is the angle between the dipole orientation $\mathbf{n}_\mu$ and the liquid crystal director $\mathbf{n}_L$, and σ determines the quality of the alignment. If σ tends towards 0, the alignment and dichroism of the dye molecules become nearly perfect; for larger σ, though, the dye molecule's orientation distribution tends towards arbitrary orientation. Importantly, a dipole with orientation $\mathbf{n}_\mu$ is equivalent to a dipole with orientation $-\mathbf{n}_\mu$.

We have adapted the Beer-Lambert law to calculate the likelihood T that a photon travels a length l within the LSC given a probability distribution $\Pr(\beta|\sigma)$. We derived the following formula, which is dependent on the absorption cross section of the dye σ_D, the dye's molar concentration c_D and a factor Φ that incorporates the probability distribution

$$\begin{aligned} T &= \exp(-3\sigma_D c_D N_A \Phi l), \\ \Phi &= \int_0^{2\pi} \mathrm{d}\phi \int_0^{\pi} \mathrm{d}\theta \sin(\theta) \Pr(\beta(\theta,\phi)|\sigma) |\mathbf{n}_\mu(\theta,\phi) \cdot \mathbf{n}_E|^2, \end{aligned} \tag{2}$$

where N_A is the Avogadro constant, and θ and ϕ denote the inclination and azimuthal angles, respectively. For homeotropic alignment and the zenith direction being normal to the top surface, β would be equal to θ. If isotropic alignment (i.e., $\Pr(\beta) = (4\pi)^{-1}$) is assumed, Eq. (2) becomes the well known Beer-Lambert law.

To circumvent the low absorption of homeotropically aligned dye molecules for normally incident light, two different dye molecules are linked together to make use of FRET. One type of dye molecule serves as an *absorption dye* or *donor*. The absorption dye can either be non-dichroic or have the polarization axis orthogonal to the alignment direction to efficiently absorb incoming sunlight. Following the absorption, it transfers the energy to the second type of dye molecule, the *emission dye* or *acceptor*, through FRET. The dichroic emission dye is aligned homeotropically and emits most of the energy outside of the escape cone. In addition to the improved absorption, it has also been shown that linked fluorophores can exhibit a better alignment than a single fluorophore within a liquid crystal host.[29] Examples of non-dichroic fluorophores include quantum dots or Rhodamine B and commonly used dichroic fluorophores are Coumarin 6 or DCM.[14,17]

The energy transfer efficiency E from donor to acceptor and the Förster radius R_0 are given by[26]

$$\begin{aligned} E &= \frac{1}{1+(R/R_0)^6}, \\ R_0^6 &= \frac{9\kappa^2 q}{128\pi^5} \int_0^{\infty} \frac{f_D(\lambda)\sigma_A(\lambda)\lambda^4}{n(\lambda)^4} \mathrm{d}\lambda \end{aligned} \tag{3}$$

with R, q, f_D, σ_A, n being the distance between the two dye molecules, the quantum yield of the donor, the fluorescence

probability of the donor, the absorption cross section of the acceptor, and the refractive index of the host medium, respectively. The factor κ^2 is given by[26]

$$\kappa^2 = (\mathbf{n}_A \cdot \mathbf{n}_D - 3(\mathbf{n}_R \cdot \mathbf{n}_D)(\mathbf{n}_R \cdot \mathbf{n}_A))^2, \quad (4)$$

where $\mathbf{n}_A$ and $\mathbf{n}_D$ are the polarizability axis unit vectors of the acceptor and the donor, respectively, and $\mathbf{n}_R$ is the unit vector pointing from the donor to the acceptor. Equation (4) would imply that no energy transfer would occur for orthogonally oriented donor/acceptor pairs. However, it has been shown experimentally that even at this configuration near-unity efficient energy transfer between rigidly linked fluorophores does occur.[30] This is because the dipoles of the fluorophores reorient themselves and, thus, break the orthogonal orientation at a much higher rate than the energy transfer rate.[30] Therefore, we assume the orientational average $\langle \kappa^2 \rangle = \frac{2}{3}$, which is common practice in FRET simulations.[31]

One important factor of FRET is the gap between the wavelength bands of the donor and acceptor over which they absorb and emit, as the transfer efficiency in Eq. (3) is dependent on the overlap of the emission probability (donor) and the absorption cross section (acceptor). We will denote the wavelength difference between the absorption maxima of both dyes the *absorption peaks separation*. Figure 2 shows the absorption and emission spectra of an acceptor and a donor dye with an absorption peaks separation of 200 nm. For both the acceptor and the donor, we use the spectral information of Coumarin 6,[32] as the spectra of organic dyes commonly used for LSCs are similar apart from the wavelength range at which they absorb and emit. Commonly used organic dye molecules include Lumogen F Red 305, Lumogen F Orange 240, Rhodamine B, DCM, and K160 among others.[5,9,14,16] For the acceptor, the absorption and emission spectra are shifted to longer wavelengths by the absorption peaks separation. The spectra of Coumarin 6 are used to demonstrate the potential of aligned dye molecule LSCs, but the model allows one to simulate the spectra of any fluorophore. This is demonstrated in Sec. IV D when Coumarin 6 is replaced with a quantum dot as donor dye. Unless stated otherwise, we assume a quantum efficiency of 80% for Coumarin 6 inside a plastic host.[33]

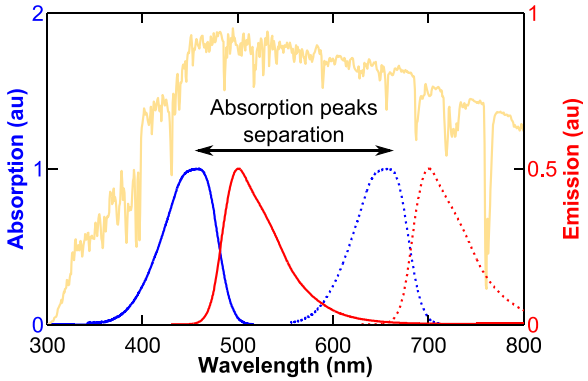

FIG. 2. Absorption (blue) and emission (red) spectra of a donor (solid) and an acceptor (dashed) dye molecule with an absorption peaks separation of 200 nm.[32] The AM1.5G spectrum is shown in yellow as a comparison.[34]

III. MONTE-CARLO RAY TRACER

We have developed a Monte-Carlo ray tracer to compute the optical efficiency $\eta_{\text{opt}}(\lambda)$ of the investigated LSC design. The optical efficiency is commonly used to assess the performance of a LSC. It is given by dividing the total number of photons reaching a solar cell by the total number of photons incident on the LSC as a function of the incoming light's wavelength. After the ray tracer determines the optical efficiency as a function of wavelength, we calculate the AM1.5G normalized optical efficiency $\bar{\eta}_{\text{opt}}$ as a wavelength independent metric to compare different LSC designs

$$\eta_{\text{opt}}(\lambda) = \frac{P_{\text{cell}}(\lambda)}{P_{\text{top}}(\lambda)}, \qquad \bar{\eta}_{\text{opt}} = \frac{\int_{\lambda_1}^{\lambda_2} A(\lambda)\eta_{\text{opt}}(\lambda)\mathrm{d}\lambda}{\int_{\lambda_1}^{\lambda_2} A(\lambda)\mathrm{d}\lambda}, \quad (5)$$

where P_{cell}, P_{top}, and $A(\lambda)$ are the power reaching the solar cells, the power incident on the top surface and the AM1.5G spectrum,[34] respectively. The limits λ_1 and λ_2 are equal to 280 nm and 4000 nm to incorporate the entire AM1.5G spectrum. As recommended by a recent LSC review, we opted to use the normalized optical efficiency as the main metric instead of an electron-generation efficiency.[2] This way the efficiency of the LSC is not dependent on the choice of the solar cell. However, for the sake of completeness, we present short-circuit current efficiencies of attached solar cells in Sec. IV E.

For all simulations, 100 000 photons are generated per wavelength to ensure the results vary by less than 0.1%. A convergence test determined that 6 nm is a good compromise between speed and accuracy for the wavelength resolution of the model. The photons impinge on the top surface of the LSC at normal incidence and at a random position. Assuming the solar cells are index-matched, a photon reaches the solar cell, once it hits one of the four side surfaces. Since the aim of this paper is to compare two different LSC systems, we are neglecting host absorption and scattering. This will be taken into account in the future once there is experimental information available about the differential scattering cross section of the liquid crystal.

The two investigated LSC systems are: (1) a LSC doped with a single dye that is isotropically oriented (*one-dye system*) and (2) a LSC doped with two linked dyes, where one dye is non-dichroic and the other dye is dichroic and homeotropically aligned (*two-dye system*, see Fig. 1(a)). For all dyes involved, isotropically or homeotropically aligned, the absorption and emission spectra of Coumarin 6 are used as described in Sec. II. While the only parameter left to vary for the one-dye system is its dye concentration, there are four parameters to vary for the two-dye system: the concentration of the dye complex, the quality of alignment (i.e., σ in Eq. (1)), the spatial distance between the two dyes and the absorption peaks separation between the dyes. Initially, we keep σ fixed at zero to fairly compare the two systems. This way only the absorption dye is absorbing incoming light in the two-dye system. Otherwise, the two-dye system would absorb incoming light over a wider spectrum than the one-dye system, making the results difficult to compare.

We use a random-mutation hill-climbing algorithm for the two-dye system to find a peak of the normalized optical efficiency as a function of the parameters.[35] An optimization algorithm is used as it would be inefficient to investigate every parameter set given the size of the parameter space. In brief, the random-mutation hill-climbing algorithm works as follows: Given an optical efficiency at a certain parameter set, a random vector is generated within the parameter space to change the parameters to a new value. If the optical efficiency at this new parameter set is higher, the new parameter set is accepted; otherwise, it is discarded. Subsequently, a new random vector is generated.

To ensure that our ray tracer accurately computes the efficiency of different LSC designs, we simulate previously published LSC configurations. The comparison between our and the published results are shown in Appendix.

IV. RESULTS AND DISCUSSION

A. Optimization of parameters

First the results are shown for $50 \times 50 \times 4\,\text{mm}^3$ LSCs, which are commonly investigated for small scale prototypes.[5,19] The optimum parameter set is found for the two-dye system using the optimization algorithm. Then each parameter is varied, while keeping the other parameters at their optimum value to determine the impact on the optical efficiency. Figure 3 depicts the optical efficiency (a) for both systems as a function of concentration and (b) for the two-dye system as a function of the distance between the absorption and emission dyes and the absorption peaks separation.

The normalized optical efficiencies reach an optimum of 7.3% and 9.4% at concentrations of 3×10^{-4} M and 4.2×10^{-4} M for the one-dye and the two-dye systems, respectively. The optical efficiency is most sensitive to concentration changes as it drops quickly due to high re-absorption for high concentrations or low absorption for low concentrations. In the two-dye system, the optimum distance between the dyes is 1.5 nm. For shorter distances too much energy is transferred back from the acceptor to the donor and, for longer distances, the system approaches a decoupled two-dye system. Similarly, the optical efficiency deteriorates for a small absorption peaks separation as the energy transfer from acceptor to donor is too high. However, the optical efficiency is steady between 9.3% and 9.4% over a large range from about 200 nm to 360 nm. Over this range, the energy transfer from donor to acceptor remains efficient given the optimum distance of 1.5 nm, while the same is already low from acceptor to donor. Also, for such a large absorption peaks separation, a photon emitted by an acceptor dye is unlikely to be re-absorbed by a donor dye. Beyond 360 nm, the spectral overlap is too little to promote energy transfer from the donor to the acceptor despite the close proximity of the two fluorophores. Importantly, the results in Fig. 3 will vary depending on the spectra of the chosen fluorophore.

B. Impact of LSC size on optical efficiency

Next, we investigate how the standard one-dye system and the advanced two-dye system perform at larger LSC sizes. One would expect the performance gap between the two-dye and the one-dye systems to widen even more for larger sizes as the number of re-absorption occurrences increases. This is verified by Fig. 4, which shows the normalized optical efficiencies for both systems as a function of geometrical gain (size of the top surface divided by size of the solar cells). The relative improvement of the two-dye system compared to the one-dye system increases from 29.2% for a $50 \times 50 \times 4\,\text{mm}^3$ LSC to 55.3% for a $1000 \times 1000 \times 4\,\text{mm}^3$ LSC; the largest size would be suitable for a window application. For the one-dye system, the escape cone losses increase from 23% (smallest LSC size) to 32.2% (largest LSC size) due to increased re-absorption, while this loss channel rises from 9.6% to 14.5% for the two-dye system.

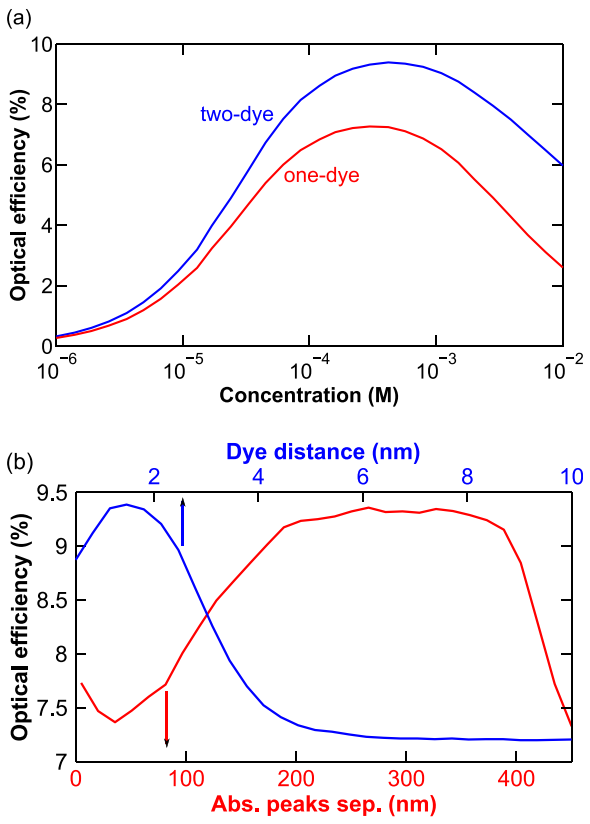

FIG. 3. Normalized optical efficiencies as a function of (a) concentration for the one-dye (red) and the two-dye system (blue) and (b) distance between dyes (blue) and absorption peaks separation (red) for the two-dye system.

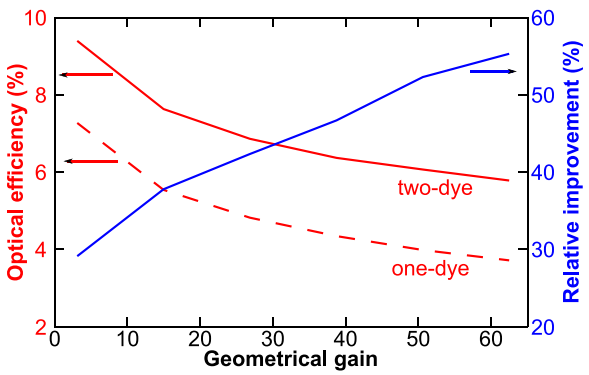

FIG. 4. Normalized optical efficiencies (red) of the two-dye (solid) and the one-dye (dashed) systems and the relative improvement (blue) as a function of gain.

The escape cone loss percentages quoted here are relative to the number of photons absorbed. The dependence on the three parameters at the largest size is similar to Fig. 3 except that the maximum is reached at a lower concentration of 1.2×10^{-4} M to limit re-absorption.

C. Investigation of different quantum yields and absorption:emission dye ratios

For the two-dye system, the non-unity quantum yield is the main loss channel as 42.3% of all absorbed photons are lost to heat for the largest size. Figure 5 shows the impact of a higher quantum yield for both dye molecules on the optical efficiency for a $1000 \times 1000 \times 4\,\text{mm}^3$ LSC. The normalized optical efficiency increases from 5.8% for a quantum yield of 80% to 7.6% and 10.3% for quantum yields of 90% and 100%, respectively. Compared to the one-dye system, this represents a relative improvement of 67.3% and 82.9%. Due to the high re-absorption probability at such large LSC sizes, the quantum yield is, as always, a crucial factor of LSC performance.

Another potential improvement to the optical efficiency would be to link multiple absorption dye molecules to one single emission dye (see Fig. 1(b)). This means the concentration of the emission dye is halved or even quartered compared to the concentration of the absorption dye. This would reduce the risk of re-absorption by the emission dye, while keeping the absorption of incoming light at the same level. Figure 5 depicts the optical efficiencies for a $1000 \times 1000 \times 4\,\text{mm}^3$ LSC with a quantum yield of 100% and absorption:emission dye ratios of 2:1 and 4:1. This would further improve the normalized optical efficiency to 11.2% (2:1) and 12% (4:1).

So far the quantum yield was assumed to be the same for both the absorption and the emission dye. However, the quantum yield of the absorption dye is not as crucial due to the efficiency of FRET. At the largest considered size, a ratio of 1:1 and an emission dye quantum yield of 100%, the normalized optical efficiency decreases only slightly from 10.3% to 9.7% if the quantum yield of the absorption dye is lowered from 100% to 50%. This is due to the energy transfer efficiency, Eq. (3), changing only marginally from 95.4% to 91.3% given a dye distance of 1.8 nm and an absorption peaks separation of 309 nm. If instead, the emission dye's quantum yield is changed to 50%, the normalized optical efficiency would drop to 2.3%.

D. Quantum dots and the importance of σ

We have shown that the donor's quantum yield is not as critical for the two-dye system. Also, re-absorption by the donor is limited as the photon experiences a strong red-shift due to FRET. This makes quantum dots perfect candidates for the donor fluorophore, as they often suffer from low quantum yields and high re-absorption losses but absorb over a wider wavelength band than organic dyes and are isotropic as well.[36–38] PbS quantum dots have been used previously as fluorophores for LSCs[37] and will be investigated here as potential donors in the two-dye system. They provide broadband absorption but suffer from a low quantum yield of 30%.[37] Figure 6 shows the spectra of PbS quantum dots together with an acceptor fluorophore that, as above, uses the shifted spectral information of Coumarin 6. It has been shown that the diameter will be around 2.4 nm for PbS quantum dots with a first absorption peak around 750 nm.[39] Thus, the minimum center-to-center distance between the donor and the acceptor is approximately 1.2 nm for this configuration.

In this section, we also show the impact of the alignment quality σ in Eq. (1) on the normalized optical efficiency using the new PbS configuration and the previously used LSC doped with Coumarin 6 as the donor fluorophore. Again, the optimum parameter set is found using the random-mutation hill-climbing algorithm for a LSC size of $1000 \times 1000 \times 4\,\text{mm}^3$. In Fig. 7, σ is varied from 0 (perfect homeotropic alignment) to 1 (close to random alignment), while keeping the other parameters at their optimum values. The area plots show the fate of the incoming photons normalized with respect to the AM1.5G spectrum. The photons are either lost through the escape cone after being absorbed (red), lost due to a non-unity quantum yield (yellow), not absorbed by a fluorophore (light blue), or picked up by the solar cell (i.e., the optical efficiency, dark blue). Importantly, the loss channels are shown here relative to the entire AM1.5G spectrum and not just all absorbed photons.

The PbS/Coumarin 6 design (27.7% at perfect alignment) is more efficient than the Coumarin 6/Coumarin 6 design

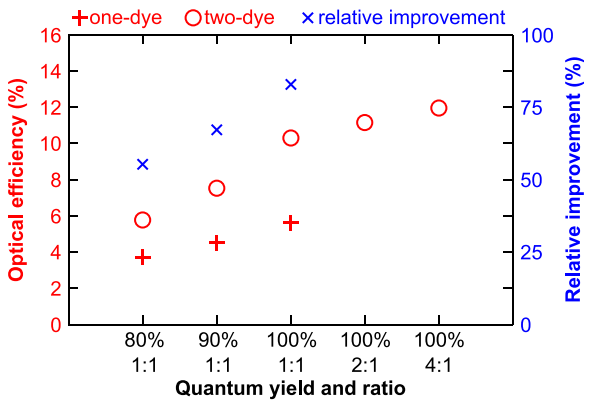

FIG. 5. Normalized optical efficiencies (red) of the two-dye (circles) and the one-dye (plus signs) systems and the relative improvement (blue crosses) as a function of quantum yield and absorption:emission dye ratio.

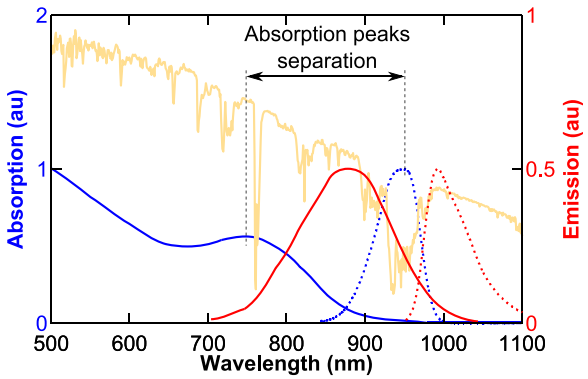

FIG. 6. Absorption (blue) and emission (red) spectra of a PbS donor (solid) and a Coumarin 6 acceptor (dashed) with an absorption peaks separation of 200 nm.[32,37] The AM1.5G spectrum is shown in yellow as a comparison.[34]

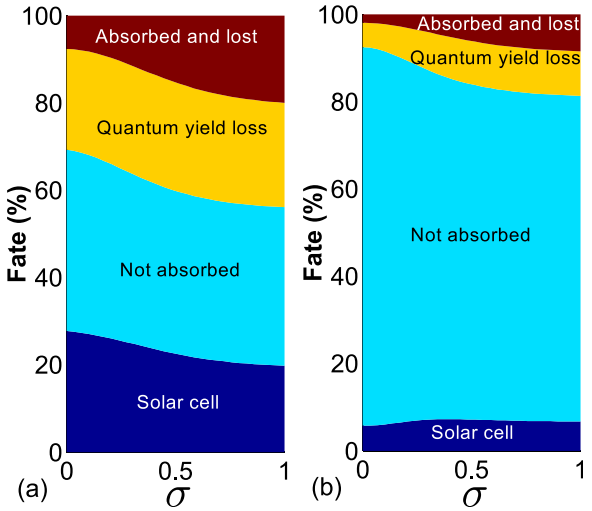

FIG. 7. Area plot for fate of incident photons for the (a) PbS/Coumarin 6 and (b) Coumarin 6/Coumarin 6 configurations. Photons are either lost through the escape cone after being absorbed (red), lost due to a non-unity quantum yield (yellow), not absorbed by a fluorophore (light blue), or picked up by the solar cell (dark blue). The results are normalized with respect to the AM1.5G spectrum.

(5.8%) as the donor fluorophore absorbs over a much wider wavelength band. The PbS quantum dot absorbs until about 950 nm, which accounts for about 71% of the AM1.5G spectrum. Interestingly, the efficiency improves at first for the Coumarin 6/Coumarin 6 design if the acceptor/emission dye alignment worsens (i.e., σ becomes larger). This is due to the emission dye absorbing much stronger incoming light for worse alignment. The stronger absorption counteracts the deteriorated trapping efficiency, which matches previous results.[16] For the PbS design, though, the optical efficiency drops for worse acceptor alignment as the wavelength band over which the acceptor dye absorbs is small compared to the absorption band of the PbS quantum dot (see Fig. 6). Thus, the additional absorption by the acceptor does not offset the deteriorated trapping efficiency anymore. The normalized optical efficiency decreases to 19.8% for a σ of unity. Hence, aligning the emission dye molecules yields a relative improvement of 39.8%. This is due to the share of photons lost due to the escape cone increasing from 7.7% to 20%. In comparison, a LSC of the same size doped solely with PbS quantum dots would achieve a maximum normalized optical efficiency of only 1.1% due to the low quantum yield and the strong overlap of the absorption and emission spectrum.

To further demonstrate the efficiency enhancement of our two-dye system, we compare it with an existing system in the literature.[40] The LSC parameters used in the other study should be similar to the ones we use as optical efficiencies will vary strongly depending on the used LSC size, fluorophore, concentration of the fluorophore, and wavelength range (i.e., λ_1 and λ_2 in Eq. (5)). A previous study investigated LSCs doped with PbSe quantum dots, which have a quantum yield of 40%.[40] For a $300 \times 300 \times 2.5\,\text{mm}^3$ sized LSC doped solely with PbSe quantum dots, a normalized optical efficiency of 2.6% was reported.[40] We simulate a LSC of the same dimensions doped solely with PbS quantum dots, which have a narrower absorption band than PbSe quantum dots and a quantum yield of 30%. Our ray tracer predicts a normalized optical efficiency of 1.7%, due to the inferior quantum yield and narrower absorption band. If we assume the PbS quantum dots have a quantum yield of 40%, the computed normalized optical efficiency is 2.4%, with the narrower absorption band accounting for the small difference to the reported 2.6%. Adding an emission/acceptor fluorophore to the system (and assuming again a quantum efficiency of 30% for the PbS quantum dots) increases the normalized optical efficiency to 31.6%, a 12-fold improvement. This is due to the lower reabsorption probability, higher quantum yield, and alignment of the added emission/acceptor fluorophore.

E. Solar cells

Until now, the optical efficiency has been used as the main metric without considering efficiencies of solar cells. Here, we additionally incorporate solar cells by comparing the short-circuit currents generated by the solar cells attached to the waveguide (I_{LSC}) and the same solar cells illuminated without the waveguide (I_{PV}). The ratio $\frac{I_{\text{LSC}}}{I_{\text{PV}}}$ yields the benefit of using a waveguide instead of just the solar cells; a value above 1 indicates that the LSC is more efficient than the solar cells by themselves, while a value below 1 indicates that there is no benefit from using the waveguide. When attaching solar cells, one has to take into account the spectrum of the photons that reach the solar cells. The solar cells should preferably have their quantum efficiency peak at the same wavelength band.

Table I presents the short-circuit currents ratio for LSC designs already investigated above. Either Silicon or Germanium solar cells are assumed for these calculations. Silicon is the most common choice for LSCs,[36,37] but the spectral response of Germanium better matches the edge emissions of some of our configurations. For the smallest investigated LSC ($50 \times 50 \times 4\,\text{mm}^3$) that is solely doped with Coumarin 6, a current ratio of only 0.2 is achieved as the top surface area of the LSC is only about three times as large as the area of the solar cells. However, for the largest size investigated and using the spectral information of Coumarin 6 for the donor and the acceptor fluorophore, the current ratio increases to 3.1. If the donor fluorophore is replaced with a PbS quantum dot, the same metric reaches a value of 8.5. Replacing Coumarin 6 with PbS quantum dots does not improve the current ratio as strongly as it improves the optical efficiency (increases from 5.8% to 27.7%). This is due to the

TABLE I. Short-circuit current ratios for different LSC configurations that have either Silicon (Si) or Germanium (Ge) solar cells attached to the sides of the LSC. The assumed quantum efficiency is specified next to the name of the fluorophore and the dimension (Dim.) indicates the top surface area of the LSC.

Dim. (m^2)	Donor	Acceptor	$\bar{\eta}_{\text{opt}}$	$\frac{I_{\text{LSC}}}{I_{\text{PV}}}$
0.05×0.05	Coum. 6 (80)	n/a	7.3%	Si: 0.2
1×1	Coum. 6 (80)	n/a	3.7%	Si: 2.0
1×1	Coum. 6 (80)	Coum. 6 (80)	5.8%	Si: 3.1
1×1	PbS QD (30)	n/a	1.1%	Si: 0.7
1×1	PbS QD (30)	Coum. 6 (80)	27.7%	Si: 8.5
1×1	PbS QD (30)	Coum. 6 (80)	27.7%	Ge: 22.5

quantum efficiency of Silicon dropping off around the spectral peak (~1050 nm) of the photons reaching the solar cells in the PbS configuration. Replacing the Silicon solar cell with a Germanium solar cell would increase the short-circuit current ratio to 22.5. This improvement is not only due to a better match between the Germanium cell and the spectral distribution of the photons reaching the solar cell, but also due to the lower short-circuit current of the Germanium cell compared to the Silicon cell. This shows how vital it is to choose a solar cell material with the appropriate spectral response to maximize the efficiency of the entire device.

V. CONCLUSION

We have shown that aligned dye molecules combined with FRET can strongly improve the optical efficiency of a LSC. The enhancement becomes even more dominant for larger LSC sizes and higher quantum efficiencies. For a $1000 \times 1000 \times 4\,mm^3$ sized LSC and a quantum efficiency of 100%, the two-dye system using two organic dyes outperforms the standard isotropic design by 82.9%. Even for a quantum efficiency of 80%, the improvement is still high at 55.3%. While the optimum dye concentration of the two-dye system varies with size, the optimum dye distance remains between 1.5 and 2 nm. Also the absorption peaks separation shows little dependence on size and, for the given spectra and dye distances, should be between 200 nm and 360 nm.

Although it is essential to choose an emission dye with a very high quantum yield, it is less important to have an absorption dye with a high quantum yield as FRET would still occur efficiently at lower quantum yields. Additionally, re-absorption by the absorption fluorophore is limited due to the large red-shift of the energy transfer. Thus, quantum dots are a feasible absorption fluorophore for this design. A $1000 \times 1000 \times 4\,mm^3$ sized LSC doped only with PbS quantum dots reaches a normalized optical efficiency of just 1.1% due to the low quantum yield and strong re-absorption. However, if the same type of quantum dot is combined with Coumarin 6 as an aligned emission dye, the normalized optical efficiency increases to 27.7% for perfect alignment. Even for random alignment, the normalized optical efficiency is still substantially larger at 19.8% than the single fluorophore system as FRET ensures that the energy is transferred efficiently to the emission dye instead of being lost to heat.

ACKNOWLEDGMENTS

This work was supported by the European Union Framework Programme 7 (FP7) via a Marie-Curie Career Integration Grant, Project No. 293567. We also acknowledge financial support from UCL BEAMS School via a Ph.D. Impact Award.

APPENDIX: MODEL VALIDATION

To validate our Monte-Carlo ray tracer, we simulate different LSC designs investigated already in previous publications, which include both modeling and experimental works.[37,40,41] The parameters of each LSC design are shown in Table II.

TABLE II. LSC design parameters of different LSC studies used for model validation.

	Dimension (mm^3)	Fluorophore	QY	Ref.
#1	$300 \times 300 \times 3$	Lumogen R305	100%	41
#2	$100 \times 100 \times 3$	Lumogen R305	100%	41
#3	$300 \times 300 \times 2.5$	PbSe QD	40%	40
#4	$300 \times 300 \times 2.5$	PbSe QD	80%	40
#5	$300 \times 300 \times 5$	PbSe QD	40%	40
#6	$300 \times 300 \times 5$	PbSe QD	80%	40
#7	$300 \times 300 \times 10$	PbSe QD	40%	40
#8	$300 \times 300 \times 10$	PbSe QD	80%	40
#9	$45 \times 12 \times 4$	PbS QD	30%	37

The published optical efficiencies of the different LSC designs and the results computed by our ray tracer are shown in Fig. 8. For the first 2 designs, the optical efficiencies quoted are equal to the number of photons reaching the solar cell divided by the number of absorbed photons.[41] As a result, they are considerably higher than the other optical efficiencies shown, which are derived using Eq. (5). The close match of our simulated results and the published results indicates that our ray tracer can accurately compute the optical efficiency of various LSC designs.

Additionally, we verify that the dye alignment and FRET algorithms used by our ray tracer yield the expected results. Figure 9 shows the trapping efficiency as a function of σ. The trapping efficiency is given by the number of photons emitted into guided modes divided by all absorbed photons. At perfect alignment about 91% of all absorbed photons are emitted into a guided mode, which matches previous theoretical findings for a waveguide with a refractive index of 1.5.[17] The trapping efficiency converges towards 75%, if σ increases as for higher values of σ, the dye molecule orientation becomes random. For random dye orientation, the remaining 25% will be emitted within the escape cone as mentioned in Sec. I.

Figure 9 also depicts the energy transfer efficiency (Eq. (3)) between a fluorescein molecule (donor) and an Alexa Fluor 532 molecule (acceptor). It compares the results of our ray tracer and previously published data and verifies that the energy transfer is computed accurately.

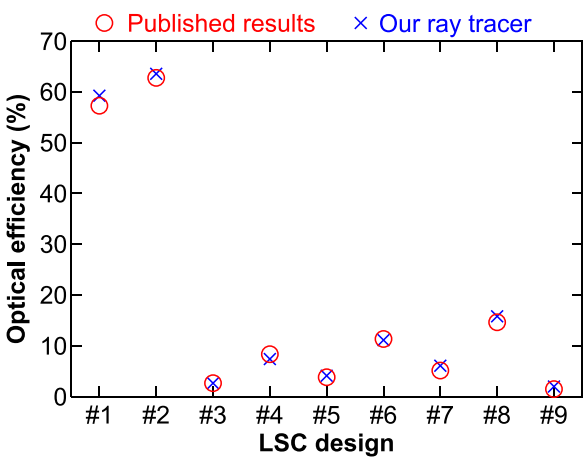

FIG. 8. Comparison between published LSC efficiencies and the results of our ray tracer using the parameters shown in Table II.[37,40,41]

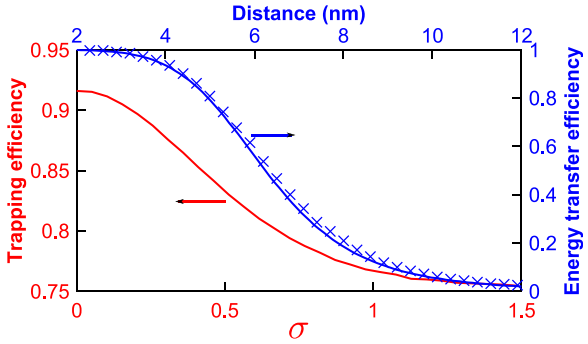

FIG. 9. Trapping efficiency (red) as a function of σ and energy transfer efficiency (blue) between fluorescein (donor) and Alexa Fluor 523 (acceptor) as a function of distance between the molecules. The energy transfer computed by our ray tracer (solid) is compared to previous findings (crosses).[26]

[1]M. J. Currie, J. K. Mapel, T. D. Heidel, S. Goffri, and M. A. Baldo, Science **321**, 226 (2008).
[2]M. G. Debije and P. P. C. Verbunt, Adv. Energy Mater. **2**, 12 (2012).
[3]W. H. Weber and J. Lambe, Appl. Opt. **15**, 2299 (1976).
[4]A. Goetzberger and W. Greube, Appl. Phys. **14**, 123 (1977).
[5]W. G. J. H. M. van Sark, K. W. J. Barnham, L. H. Slooff, A. J. Chatten, A. Büchtemann, A. Meyer, S. J. McCormack, R. Koole, D. J. Farrell, R. Bose, E. E. Bende, A. R. Burgers, T. Budel, J. Quilitz, M. Kennedy, T. Meyer, C. D. M. Donegá, A. Meijerink, and D. Vanmaekelbergh, Opt. Express **16**, 21773 (2008).
[6]T. Markvart, J. Appl. Phys. **99**, 026101 (2006).
[7]U. Rau, F. Einsele, and G. C. Glaeser, Appl. Phys. Lett. **87**, 171101 (2005).
[8]M. G. Debije, M. P. Van, P. P. Verbunt, M. J. Kastelijn, R. H. van der Blom, D. J. Broer, and C. W. Bastiaansen, Appl. Opt. **49**, 745 (2010).
[9]R. Reisfeld, Opt. Mater. **32**, 850 (2010).
[10]S. Chandra, J. Doran, S. J. McCormack, M. Kennedy, and A. J. Chatten, Sol. Energy Mater. Sol. Cells **98**, 385 (2012).
[11]H. R. Wilson, Sol. Energy Mater. **16**, 223 (1987).
[12]C. Tummeltshammer, M. S. Brown, A. Taylor, A. J. Kenyon, and I. Papakonstantinou, Opt. Express **21**, A735 (2013).
[13]K. Barnham, J. L. Marques, J. Hassard, and P. O'Brien, Appl. Phys. Lett. **76**, 1197 (2000).
[14]P. P. C. Verbunt, A. Kaiser, K. Hermans, C. W. M. Bastiaansen, D. J. Broer, and M. G. Debije, Adv. Funct. Mater. **19**, 2714 (2009).
[15]R. W. MacQueen, Y. Y. Cheng, R. G. C. R. Clady, and T. W. Schmidt, Opt. Express **18**, A161 (2010).
[16]M. G. Debije, Adv. Funct. Mater. **20**, 1498 (2010).
[17]C. L. Mulder, P. D. Reusswig, A. M. Velázquez, H. Kim, C. Rotschild, and M. A. Baldo, Opt. Express **18**, A79 (2010).
[18]C. L. Mulder, P. D. Reusswig, A. P. Beyler, H. Kim, C. Rotschild, and M. A. Baldo, Opt. Express **18**, A91 (2010).
[19]M. G. Debije, P. P. C. Verbunt, B. C. Rowan, B. S. Richards, and T. L. Hoeks, Appl. Opt. **47**, 6763 (2008).
[20]R. W. MacQueen and T. W. Schmidt, J. Phys. Chem. Lett. **4**, 2874 (2013).
[21]W. E. Benjamin, D. R. Veit, M. J. Perkins, E. Bain, K. Scharnhorst, S. McDowall, D. L. Patrick, and J. D. Gilbertson, Chem. Mater. **26**, 1291 (2014).
[22]J. ter Schiphorst, A. M. Kendhale, M. G. Debije, C. Menelaou, L. M. Herz, and A. P. H. J. Schenning, Chem. Mater. **26**, 3876 (2014).
[23]D. Sahin, B. Ilan, and D. F. Kelley, J. Appl. Phys. **110**, 033108 (2011).
[24]A. R. Burgers, L. H. Slooff, R. Kinderman, and J. A. M. van Roosmalen, in Proceedings of the 20th European Photovoltaic Solar Energy Conference, Barcelona, June, 2005.
[25]J. Sansregret, J. M. Drake, W. R. L. Thomas, and M. L. Lesiecki, Appl. Opt. **22**, 573 (1983).
[26]L. Novotny and B. Hecht, *Principles of Nano-Optics* (Cambridge University Press, Cambridge, 2006).
[27]J. D. Jackson, *Classical Electrodynamics* (Wiley, New York, 1999).
[28]J. A. Rice, *Mathematical Statistics and Data Analysis* (Duxbury, Belmont, 1995).
[29]A. M. Kendhale, A. P. H. J. Schenning, and M. G. Debije, J. Mater. Chem. A **1**, 229 (2013).
[30]H. Langhals, A. J. Esterbauer, A. Walter, E. Riedle, and I. Pugliesi, J. Am. Chem. Soc. **132**, 16777 (2010).
[31]B. W. van der Meer, Rev. Mol. Biotechnol. **82**, 181 (2002).
[32]Oregon Medical Laser Center, "Coumarin 6," see http://omlc.ogi.edu/spectra/PhotochemCAD/html/013.html (2014).
[33]G. A. Reynolds and K. H. Drexhage, Opt. Commun. **13**, 222 (1975).
[34]National Renewable Energy Laboratory, "Reference Solar Spectral Irradiance: Air Mass 1.5," see http://rredc.nrel.gov/solar/spectra/am1.5/ (2013).
[35]S. Forrest and M. Mitchell, in *Foundations of Genetic Algorithms*, edited by D. Whitley (Morgan Kaufmann, San Mateo, CA, 1993), Vol. 2, pp. 109–126.
[36]V. Sholin, J. D. Olson, and S. A. Carter, J. Appl. Phys. **101**, 123114 (2007).
[37]G. V. Shcherbatyuk, R. H. Inman, C. Wang, R. Winston, and S. Ghosh, Appl. Phys. Lett. **96**, 191901 (2010).
[38]M. Kennedy, S. J. McCormack, J. Doran, and B. Norton, Sol. Energy **83**, 978 (2009).
[39]I. Moreels, K. Lambert, D. Smeets, D. De Muynck, T. Nollet, J. C. Martins, F. Vanhaecke, A. Vantomme, C. Delerue, G. Allan, and Z. Hens, ACS Nano **3**, 3023 (2009).
[40]S. R. Wilton, M. R. Fetterman, J. J. Low, G. You, Z. Jiang, and J. Xu, Opt. Express **22**, A35 (2014).
[41]L. R. Wilson, B. C. Rowan, N. Robertson, O. Moudam, A. C. Jones, and B. S. Richards, Appl. Opt. **49**, 1651 (2010).